Materials Advances

ROYAL SOCIETY OF CHEMISTRY

PAPER

View Article Online
View Journal | View Issue

Cite this: *Mater. Adv.*, 2020, **1**, 1930

Styrene-*co*-DVB grafted PVDF proton exchange membranes for vanadium redox flow battery applications†

Abhishek Rajput,[ab] Harun Khan,[c] Savan K. Raj,[ab] R. Kothandaraman*[c] and Vaibhav Kulshrestha *[a]

Received 10th July 2020,
Accepted 4th August 2020

DOI: 10.1039/d0ma00496k

rsc.li/materials-advances

Styrene–DVB copolymer grafted semi-interpenetrating type PVDF-based proton exchange membranes (PEMs) have been designed for vanadium redox flow battery (VRFB) applications. The PEM contains separate regions for the proton conduction *via* hydrophilic channels, whereas mechanical stability is maintained by the hydrophobic part present in the membrane matrix. Mechanical, thermal, and oxidative stabilities of the membranes are investigated. The VRFB test was conducted at 50 mA cm^{-2} and 100 mA cm^{-2} current densities. The HA-45 membrane displays better performance than the HA-35 membrane. The HA-45 membrane exhibits an excellent peak current density of 470 mA cm^{-2} and a power density of 336 mW cm^{-2}. With the HA-45 membrane, a specific capacity of 20.30 and 21.11 A h L^{-1} was realized at 100 mA cm^{-2}, and 50 mA cm^{-2}, respectively, and they are comparable to the theoretical capacity of 26.8 A h L^{-1}. This was possible due to the reduced crossover of vanadium ions through the membrane. The energy efficiency for the HA-45 membrane is 80% which is equivalent to that using Nafion 117 at 100 mA cm^{-2} current density. From these results, HA-45 is found to be a suitable membrane for VRFB applications.

1. Introduction

The demand for energy is rising every day all over the world, and the natural resources will become extinct in the near future,[1–8] and so there is a need to address the generation of energy without harming the environment. The energy share of renewable sources such as wind and solar is increasing in the grid. As these sources are seasonal, there is a need for an associated electrical energy storage system for sufficient load leveling off the grid. Vanadium electrolytes have great potential for this due to their long life span and minimal environmental impact, the minimum required cell voltage for application, and the fact that they are flexible in operation.[9–11] The vanadium redox flow battery (VRFB) is an electrochemical, electrical storage energy system that stores energy in the form of electroactive materials in large electrolyte reservoirs.[12–16] The VRFB consists of two electrolyte compartments separated by an ion exchange membrane (IEM), which acts as a barrier to avoid the intermixing of the electrolyte solution, and carbon felt in contact with the membrane and the current collector carries out the redox transformations during the charging/discharging of the VRFB. The redox couples are VO_2^+/VO^{2+} and V^{3+}/V^{2+} in the anolyte and catholyte compartment, respectively.[17] The IEMs required for VRFB should possess good mechanical and chemical stability, together with good proton conductivity and low crossover of vanadium ions.[18,19] Nafion is the state-of-the-art membrane used for redox flow batteries possessing good proton conductivity and mechanical stability. The high cost of vanadium and Nafion are significant disadvantages for the commercialization of VRFB.[20–24]

The sulfonated aromatic polymer membranes tend to be low cost, chemical resistant, and have good proton conductivity. Sulfonated poly(ether ether ketone) (SPEEK) and sulfonated poly(ether sulfone) (SPES) based membranes have been studied at optimized functionalization for VRFB application.[25–27] The poly(vinylidene fluoride)-*g*-poly(styrenesulfonic acid) (PVDF-*g*-PSSA) and branched sulfonated poly(fluorenyl ether ketone sulfone)s based cation exchange membranes (CEMs) were also studied for use as effective separators for VRFB.[28–30] Blended membranes such as Nafion/polyvinylidene, and SPEEK/PVDF were studied for improved selectivity.[31,32] Commercial perfluorosulfonic membranes with different ion exchange capacities were also studied for their applicability in VRFB, because membrane

[a] *CSIR-Central Salt and Marine Chemicals Research Institute (CSIR-CSMCRI), Council of Scientific & Industrial Research (CSIR), Gijubhai Badheka Marg, Bhavnagar 364 002, India. E-mail: vaibhavk@csmcri.res.in, vaibhavphy@gmail.com*

[b] *Department of Physics, The MK Bhavnagar University, Bhavnagar 364 002, India*

[c] *Department of Chemistry, Indian Institute of Technology Madras, Chennai 600036, India. E-mail: rkraman@iitm.ac.in*

† Electronic supplementary information (ESI) available: The chemical, structural, physicochemical characterization and membrane stability are included in Sections S1–S3. Fig. S1–S4 and Tables S1 and S2. See DOI: 10.1039/d0ma00496k

ion-exchange capacity affects the VRFB performance, however, the effect of polymer molecular architecture on the size of the hydrophilic domains also affects the membrane transport properties.[33] Anion exchange membranes (AEMs) also show a long life cyclic ability in VRFB due to the Donnan exclusion principle, which is responsible for low vanadium crossover but also suffers due to low ionic conductivity.[26] Crosslinked PEEK, SPEEK, and polyetherimide (PEI) based zwitterionic membranes showed high ionic conductivity, minimal vanadium permeability, enhanced mechanical strength, and chemical inertness for the VRFB application.[34,35] The vanadium crossover of the membranes was addressed by reducing free volume using a nano-filler, which also enhanced mechanical stability and showed a blocking effect for vanadium ions across the membrane.[36] Modified Nafion membrane has also been studied for the VRFB application using different techniques.[37–39] Due to the highly oxidative and reducing environment of the catholyte and anolyte in the VRFB it is very difficult to sustain the stability of the membrane as there may be a possibility of leaching of the fillers.[40–43] Maintaining stability of the membrane without compromising the ionic conductivity in the VRFB environment is an important parameter.

Here, the design of a semi-interpenetrating network is reported, which is based on grafting of styrene and divinyl benzene (DVB)_ in the PVDF matrix to prevent the transport (crossover) of vanadium ions between the compartments, which causes self-discharge of the VRFB. The synthesized membranes show a balance in the hydrophobic and hydrophilic regions, which is responsible for the stability and ion conduction.

2. Experimental section

2.1 Materials and method

Poly(vinylidene fluoride-*co*-hexafluoropropylene) (PVDF-HFP), styrene (St), DVB, and 2,2-azobis(isobutyronitrile) (AIBN) were obtained from Sigma-Aldrich. Sulfuric acid, chlorosulfonic acid (CSA), dimethylacetamide (DMAc), and dichloroethane (DCE) were obtained from Finar Chemicals Limited, India.

The PVDF-*co*-HFP was dehydrofluorinated using a previously reported method.[30] Co-polymerization of St and DVB with dehydrofluorinated PVDF was performed successfully using AIBN as an initiator. The reaction mixture was stirred at 110 °C for 16 h to polymerize the St and DVB with DPVDF *via* free radical polymerization. The viscous product obtained was cast on a glass plate and dried under an IR lamp to form the film. Polymer films with a thickness of 240 ± 5 μm were prepared with a predetermined copolymer composition of styrene and DVB compared to DPVDF. Further functionalization of the films was performed, to convert them into membranes, using 20% CSA and the membranes were designated as HA-35 and HA-45 as per the ratio of St and DVB as shown in Scheme 1. The prepared membranes were washed with deionized water to remove the unreacted acid.

2.2 Characterization of membranes

The samples were characterized by means of their chemical and structural properties, and details of the characterization are included in the ESI.† The thermo-mechanical stabilities of the membrane samples were evaluated by TGA and a universal

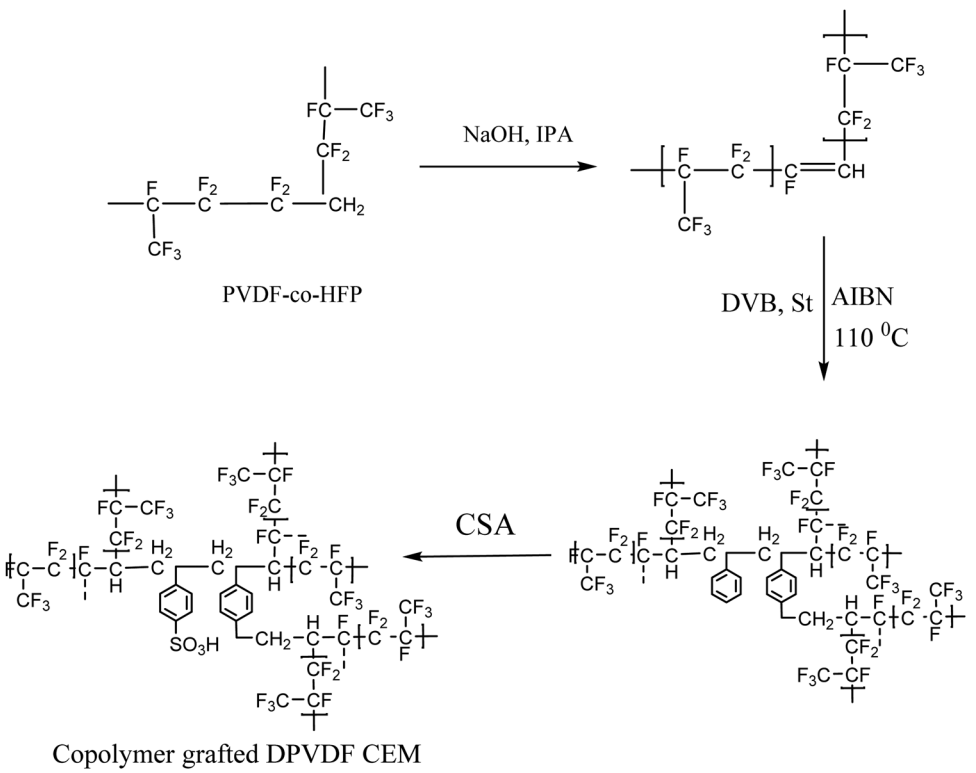

Scheme 1 Synthesis of a copolymer grafted DPVDF proton exchange membrane.

testing machine (UTM). The oxidative stability of the prepared membranes in Fenton's reagent was measured at 80 °C. Details of the characterization are included in the ESI.† A BioLogic VSP potentiostat controlled by EC-Lab software was used for electrochemical impedance spectroscopy (EIS) measurement. The EIS was performed at an open circuit potential with a V_{rms} perturbation of 10 mV in the frequency range of 200 kHz to 100 mHz. The water uptake behavior of the membranes was determined by recording the weight gain after equilibration in water for 24 h. The ion exchange capacity (IEC) was estimated from the results of acid base titration. Proton conductivity of the membranes was measured on a CH Instruments CHI-608 potentiostat/galvanostat. Details of the experiments are given in the (ESI†).[39,41]

2.3 The VO^{2+} ion permeability and VRFB single cell performance

Measuring the vanadium ion permeability of the VRFB is a crucial step for determining the cross mixing of vanadium ions during the VRFB operation. An ideal membrane should have the ability to isolate both the half-cells to avoid cross mixing. Permeability of vanadium ions was evaluated in a diffusion cell separated with a membrane. One cell was filled with a solution of 1.5 M $VOSO_4$ in 3 M H_2SO_4 while another cell was filled with 1.5 M $MgSO_4$ in 3 M H_2SO_4 solution to equalize the ionic strength and overcome the osmotic pressure. Both the solutions were continuously stirred to minimize concentration polarization at the membrane surface. Samples were collected from the cell at regular intervals and the VO^{2+} ion concentration was measured by a UV-Vis spectrometer. The VO^{2+} permeability was calculated using the following equation:

$$V_B = \frac{dC_B(t)}{dt} = A\frac{P}{L}\{C_A - C_B(t)\} \quad (1)$$

where, V_B is the volume of VO^{2+} in the right-hand cell, A is the effective area of the membrane, L is the thickness of the membrane, P is the permeability of the VO^{2+} ion, and C_A and C_B are the VO^{2+} concentrations in first and second reservoir, respectively, as a function of time.[36]

The VRFB cell performance with the prepared membranes was tested with a two compartment flow cell comprising of graphite electrodes (geometric area: 25 cm^2) and current collectors. The membrane acted as separator, and was sandwiched between graphite sheets. The twin compartment was recirculated with an electrolytic solution of $VOSO_4$ (1 M in 3 M H_2SO_4 solution) with a flow rate of 40 mL min^{-1} controlled by peristaltic pumps. The VRFB charging and discharging was performed using an Arbin Instruments CH-608E battery tester. For charge–discharge experiments, a constant current density of 50 and 100 mA cm^{-2} was applied with a 1.8 V upper voltage limit and a 0.8 V lower voltage limit. The coulombic efficiency (CE), voltage efficiency (VE), and energy efficiency (EE) of the VRFB were estimated by the following equations:

$$CE = \frac{C_{dis}}{C_{ch}} \times 100 \quad (2)$$

where C_{dis} and C_{ch} are the discharge capacity and charge capacity, respectively, which can be calculated from eqn (2) and (3).

$$C_{dis} = I_d \times t_d \quad (3)$$

$$C_{ch} = I_c \times t_c \quad (4)$$

where I_d and I_c are the current used during discharging, and charging, respectively.

$$VE = \frac{V_{dis}}{V_{ch}} \times 100 \quad (5)$$

$$V_{dis} = V_d \times t_d \quad (6)$$

$$V_{ch} = V_c \times t_c \quad (7)$$

$$EE = CE \times VE \quad (8)$$

where, V_d and V_c are the discharge and charge voltage, respectively.[17]

3. Results and discussion

3.1 Chemical, structural and morphological properties of membranes

Fig. S1 (ESI†) shows the typical ATR-IR spectra of the prepared membranes. Dehydrofluorination of PVDF-*co*-HFP was confirmed by the peak at about 1675 cm^{-1} which was due to the formation of –C═C–. Styrene was successfully confirmed by the detection of a stretching vibration associated with the C═C bond of the benzene ring at frequencies of 1394, 1447 and 1534 cm^{-1}. A vibration band at about 677 cm^{-1} was ascribed to the aromatic –CH bond deformation of a mono substituted benzene ring of the grafted styrene. For the di-substituted ring of DVB a band at about 824 cm^{-1} appeared. The bending frequency at about 834 cm^{-1} and a stretching frequency at 2920 cm^{-1} showed the presence of the aliphatic saturated –C–H– group of alkanes. Moreover, the strong stretching band in frequency range 1025–1168 cm^{-1} confirmed the presence of a sulfonic acid group in membrane matrix.[29,42]

The surface morphology of the membrane was studied using SEM analysis, and the membrane exhibits a dense and homogenous nature as shown in Fig. 1. The surface of the membrane looks porous up to the sub-micron region and facilitates the transport of protons across the membrane Fig. 1A and B. The pores are not interconnected with each other as confirmed by the cross-sectional view of the membrane Fig. 1C and D.[44] The membrane was transparent in nature and no phase separation was found in it (Fig. 2).

3.2 Stability of the membranes

Membranes were tested for their thermal and mechanical stability by TGA and UTM, respectively. Fig. S2 (ESI†) shows the TGA thermogram of the membranes, where three weight loss regions were observed. The first weight loss was at 100–150 °C and arose due to the water associated with membrane matrix. The

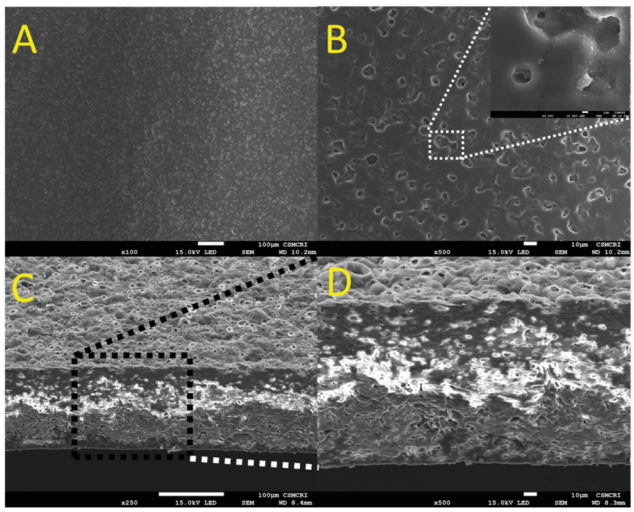

Fig. 1 Surface and cross-sectional SEM image for the prepared membrane at different magnifications.

second weight loss was due to degradation of the sulfonic acid group present in the membrane and the final weight loss at about 460 °C was due to the degradation of the main backbone of polymer.[45] The HA-45 membrane, showed a higher thermal stability than HA-35 as confirmed by the weight loss up to 460 °C. The mechanical stability of both the membranes was evaluated and the stress–strain curves are presented in Fig. S3 (ESI†). The HA-45 membrane showed higher values of strain and stress compared to the HA-35 membrane, and this may be due to the retention of more water by the HA-45 membrane, which acted as a plasticizer for the matrix which reduced the modulus of HA-45 by 25% when compared with the HA-35 membrane (Fig. S3, ESI†).[46] The oxidative stability of the membrane was also investigated by dipping the membranes into Fenton's reagent for 3 h, and then evaluating the loss in ionic conductivity. The HA-45 showed a 2% loss in stability whereas there was a 3% loss for HA-35. Here, the hydrophobic region was responsible for the stability of the membrane whereas the ionic conductivity was dependent on the hydrophilic region of the membranes.[38,47–49] The prepared membrane was stable and showed potential for the redox experiments.

3.3 Water uptake behaviour and transport properties of the membranes

Water is an essential parameter for IEMs. Water uptake for HA-35 was found to be 41.5%, and 46% for the HA-45 membrane.[41,42]

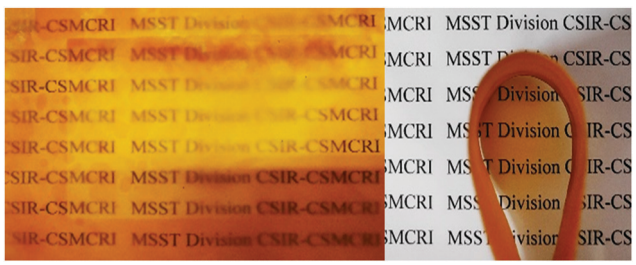

Fig. 2 Optical image for the HA-45 membrane.

The enhancement in water uptake was due to the presence of large number of functional groups in the HA-45 membrane compared to the HA-35 membrane, and the functional groups also increased water uptake (Table 1). The expansion was proportional to the water uptake, and as the water uptake increased, the membrane expansion also increased, and the valencies of hydrophobic and hydrophilic regions maintained the expansion ratio and only 22% for HA-35 and 28% for HA-45 was noted, which was quite reasonable for IEMs. The IEC is an equally important parameter for IEM, which confirmed the presence of a functional group in IEM, and about 78% enhancement noted by enhancing the 10 wt% of St–DVB in the membrane matrix. Table 1, shows the effect of variation in the copolymer content on the IEC for the semi-interpenetrating membranes, which was 1.5 meq g^{-1} for HA-35, and 2.67 meq g^{-1} for HA-45.

The ionic conductivities of the membranes are presented in Table 1, and they depend upon several factors such as the IEC, water content, density of functional groups present in the polymer matrix and so on. The ionic conductivities of the membranes increased with the increased amount of St and DVB in the membrane matrix. Incorporation of St-*co*-DVB was responsible for the formation of the dense semi-interpenetrating type network in the polymer and thus for the improved pathway for the ion transfer through wide nano channels. Thus, it improves IEC, water uptake and enhanced transport through the membranes ultimately leading to improvement in ionic conductivity. The ionic conductivity for HA-45 was found to be 6.85×10^{-2} S cm^{-1}, which was 16% higher than that of HA-35, which was 5.95×10^{-2} S cm^{-1}. The EIS measurements were also performed to assess the internal resistance of the VRFB cell. The HA-45 showed a lower internal resistance than the HA-35 due to a higher content of sulfonic acid groups being present in the membrane matrix.

3.4 Vanadium crossover resistance and single cell performance

The vanadium ion permeability with time across the membrane was calculated to determine the suitability of the membrane for a redox flow battery and is shown in Fig. 3. Membranes with a higher copolymer content showed a lower vanadium ion permeability compared to other membranes. The increase of copolymer content in the membrane matrix lead to the formation of a dense semi-interpenetrating type network, which restricted the movement of the vanadium ions and only allowed the protons through the narrow channels present. The vanadium permeation for the HA-35 membrane was found to be 30% higher than that of the HA-45 membrane (2.5×10^{-7} cm^2 min^{-1}). Ion selectivity provides vital information regarding the diffusion of protons and vanadium across the membrane as shown in Table 1, and the ionic selectivity of HA-45 membranes was found to be better than that of HA-35, and overall enhanced ionic conductivity and a very low vanadium ion crossover was responsible for the better selectivity, and HA-45 possessed a 41 times higher selectivity than HA-35. Vanadium crossover resistance and oxidative stability for the prepared membranes was found to be exceptional. The HA-45 membrane showed a

Table 1 The IEC, water uptake, expansion ratio (%), membrane cell resistance, ionic conductivity, and H^+ selectivity for the prepared membranes

Membrane	IEC (meq g^{-1})	Water uptake (%)	Expansion ratio (%)	Cell resistance (Ohms)	Ionic conductivity $\times 10^{-2}$ (S cm^{-1})	Selectivity $\times 10^5$ (S min cm^{-3})
HA-35	1.50	41.5	22.0	0.070	5.95	1.6
HA-45	2.67	46.0	28.0	0.031	6.85	2.74
Nafion 117	0.91	19.3	17.0	0.030	8.10	2.85

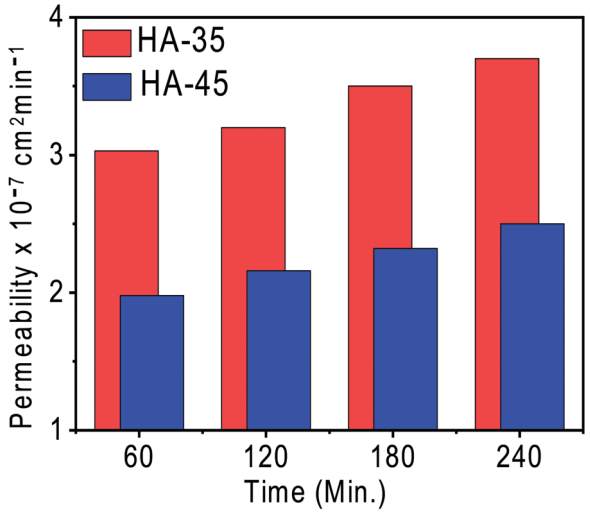

Fig. 3 Vanadium permeability for the prepared membranes.

lower permeability and higher selectivity for vanadium ions, which was suitable for the redox flow battery application.

The charging–discharging of the VRFB single cell were performed to check the suitability of semi-interpenetrating type membranes for the redox flow battery application. The VRFB cell was charged at two constant current densities of 50 mA cm^{-2} and 100 mA cm^{-2} keeping a cut off voltage of 1.8 V. The charge–discharge potential depends upon the migration of protons across the membrane from one side to other and the selectivity of the membrane, by the influence of the input current densities. Charge–discharge voltage depends mainly on three overpotentials, namely ohmic, activation, and concentration overpotentials. The membrane conductivity and the contact resistance of the VRFB determined the magnitude of the ohmic overpotential at a given current density. Hence, improving the conductivity of the membrane will reduce this overpotential. As the same electrodes are used in this study, the activation overpotential was independent of the membrane used if the vanadium crossover across the membrane is same. Because the vanadium permeability is low with the HA-45 membrane, the concentration overpotential was expected to be low for a VRFB with HA-45.

Fig. 4 shows the charge–discharge cycle of HA-45 and HA-35 membranes at 50 mA cm^{-2} current density and a comparison of the membranes at 100 mA cm^{-2}. At a higher current density, the charge–discharge cycle time was reduced, due to the fast electrochemical reaction. The HA-45 membrane showed a similar pattern of charging and discharging in a single cell as the Nafion membrane. The CE of HA-35 and HA-45 are shown in Table S1 (ESI†), the CE for the HA-35 membrane was found to be 89% and 94% at 50 mA cm^{-2} and 100 mA cm^{-2} applied current density, respectively. The HA-45 membrane had a better CE than the HA-35 membrane for both the applied current density but more difference was observed at 50 mA cm^{-2}. The EIS measurements were carried out to assess the internal resistance of the VRFB cell from the high frequency impedance value. The HA-45 showed an internal resistance of 0.031 Ohms whereas internal resistance for the HA-35 membrane was almost double (0.072 Ohm), which may be due to the presence of a higher density of sulfonic acid groups present in the HA-45 membrane matrix due to the higher content of grafted copolymer. Because HA-45 had nearly half of the internal resistance of

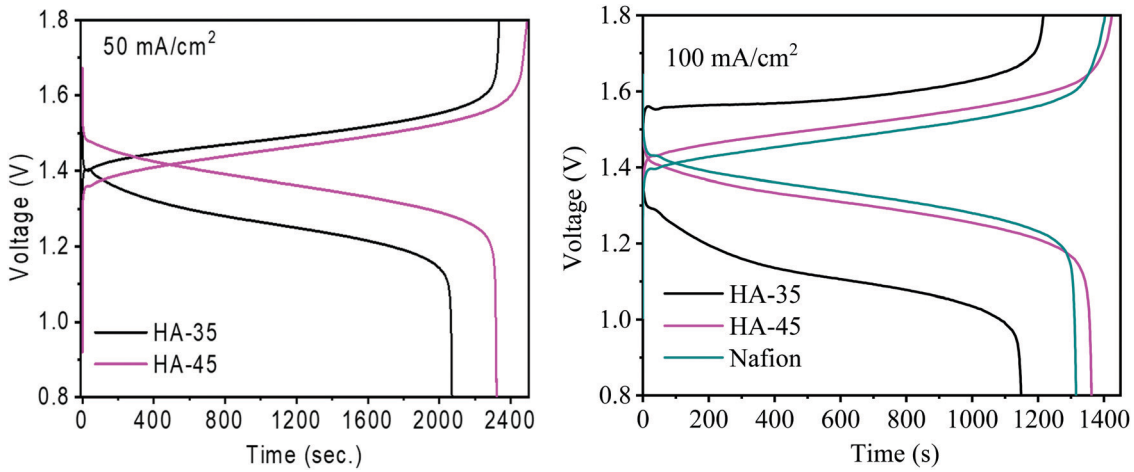

Fig. 4 Charging and discharging for single cell VRFB with HA-35, HA-45 and Nafion 117 membrane at 50 mA cm^{-2} and 100 mA cm^{-2} current density.

HA-35, HA-45 was expected to have a lower ohmic drop than HA-35, which is clearly visible in Fig. 4. The VE of the VRFB cell for the HA-45 at current densities of 50 mA cm^{-2} and 100 mA cm^{-2} was 94% and 84%, respectively, whereas for HA-35 it was 84% and 71% as shown in the Fig. 5B.

The EE is an essential performance indicator for the suitability of membrane in the energy storage system during the charge–discharge cycle with various current densities (Fig. 5C).[50] At an applied current density of 100 mA cm^{-2}, 80% of the EE value for HA-45 shows that it has potential and that it would be an effective candidate for VRFB applications. The EE for HA-45 was

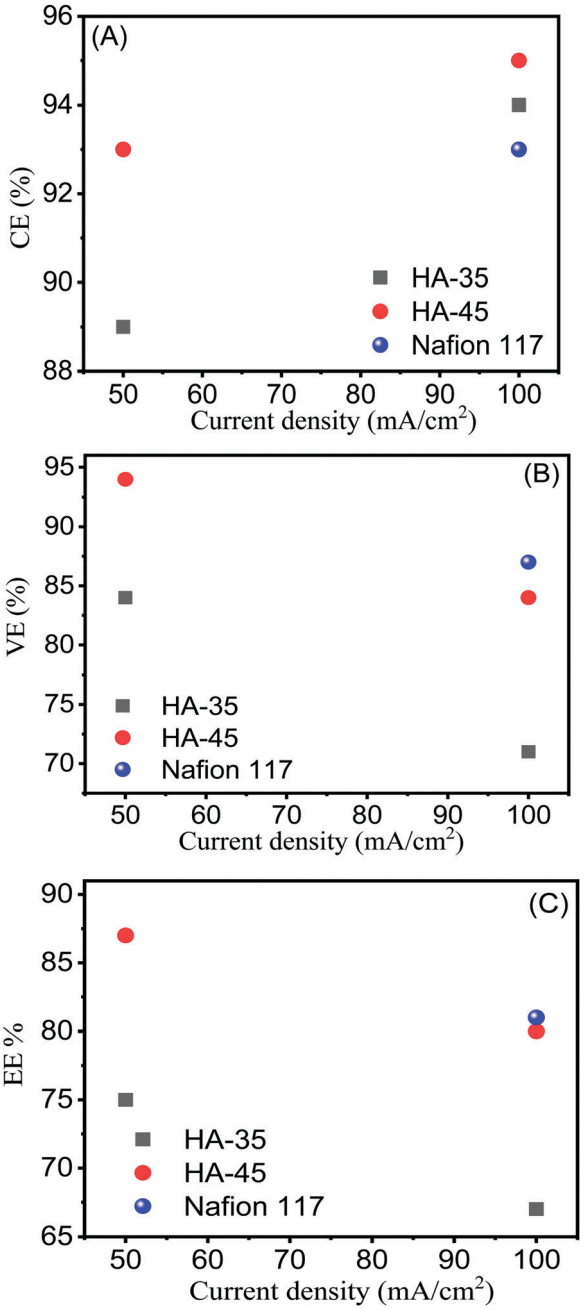

Fig. 5 Coulombic, voltage and energy efficiencies *vs.* current density for HA-35, HA-45 and Nafion 117 membranes.

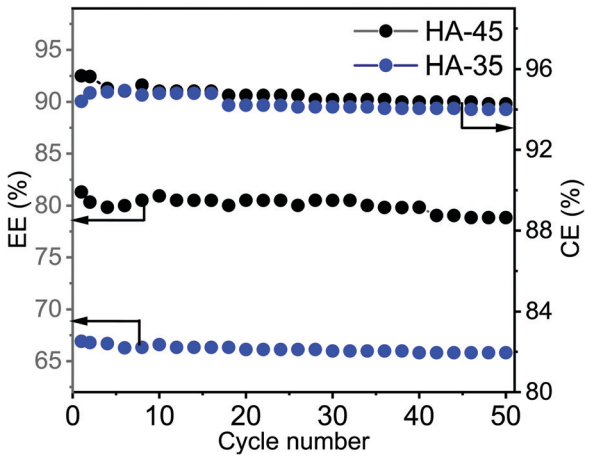

Fig. 6 Effect on EE and CE of both the membranes over a number of cycles.

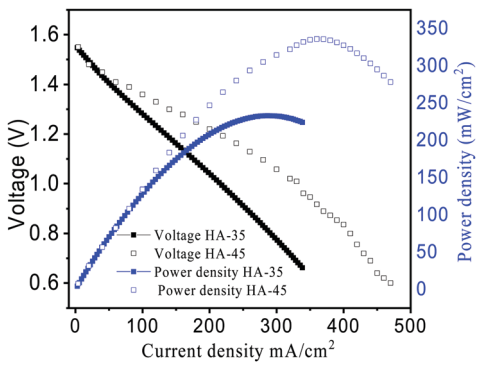

Fig. 7 Polarization curve for the prepared membranes.

superior due to the overall characteristics of the membranes, namely, low crossover of vanadium ions, good ionic conductivity, and lower cell resistance leading to reduced ohmic loss. The overall efficiency evaluation showed that the HA-35 membrane was suitable for batteries operating at lower current densities where the reduction of the vanadium crossover is essential. Conversely, the HA-45 membrane with a higher IEC is more suitable for VRFBs operating at a higher current density. The HA-45 membrane shows superior performance in all aspects, *i.e.*, CE, VE and EE, as shown in Fig. 5.[33] The results were compared with those of the state-of-the-art Nafion 117 membrane with a current density of 100 mA cm^{-2}. The EE of Nafion 117 was found to be 81%, which was equivalent to the values for the HA-45

Table 2 Comparison of capacity and specific capacity at various current densities for HA-35 and HA-45 membranes

	50 mA cm^{-2}		100 mA cm^{-2}		
Current density/ membrane	Capacity (A h)	Specific capacity (A h L^{-1})	Capacity (A h)	Specific capacity (A h L^{-1})	Theoretical specific capacity (A h L^{-1})
HA-35	0.71	17.92	0.80	19.84	26.8
HA-45	0.81	20.30	0.84	21.11	

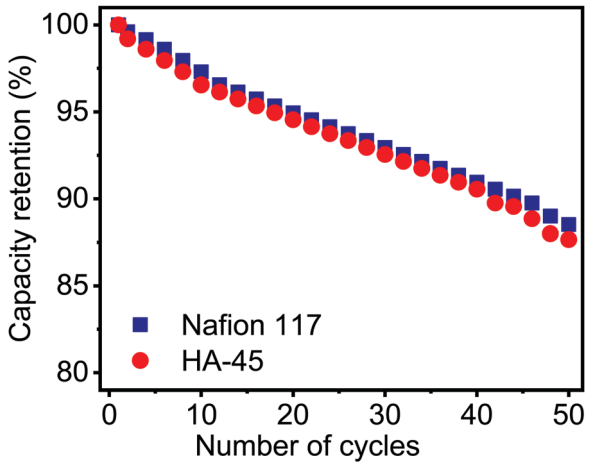

Fig. 8 Number of cycles *versus* capacity retention for HA-45 and Nafion 117 membranes.

membrane. The effect on EE and CE with the number of cycles is shown in Fig. 6. No major change was observed up to 50 cycles. No change in VE was observed when it was measured for a number of cycles, as shown in Fig. S4 (ESI†).

The peak power density for power related applications was evaluated using the polarization curve shown in Fig. 7. This polarization curve showed that the current density and power density of the cell with HA-45 was better than with the HA-35 membrane.

The power density delivered by the VRFB increased by 40% for the HA-45 membrane compared to the HA-35 membrane, as shown in Table S2 (ESI†). The polarization curve shows the capability of HA-45 to reduce the voltage loss, due its minimal vanadium crossover and good ionic conductivity compared to the HA-35. Table 2 shows the current density *vs.* capacity of VRFB for the prepared membranes. The specific capacities for the HA-45 membrane were found to be 21.11 A h L^{-1} and 20.30 A h L^{-1} at 100 and 50 mA cm^{-2}, respectively, which was near to the theoretical value of 26.8 A h L^{-1} for the 1 M vanadium electrolyte solution. Generally, the specific capacity decreased at a higher current density, and here the opposite trend was observed. This might occur due to the cumulative time reduction for the vanadium crossover.

Table 3 Comparison of the performance of the prepared membranes compared to membranes reported in the literature under similar conditions

Membranes	Vanadium permeability × 10^{-7}	CE (%)	VE (%)	EE (%)	Current density (mA cm^{-2})	Ref.
HSPAEK	5.5	92	83	77	80	28
Nafion-117	23.84	92	80	74	80	32
S/P-15	2.75	97	79	76	80	32
CrSPK45-S	0.08	98	86	85	80	34
SPEEK/PTFE	NA	93	89	83	80	51
S/GO 3	5.2	97	86	84	80	52
S/PAN-15	17.8	94	81	77	100	53
HA-45	2.5	95	84	80	100	Present study

Retention capacity *versus* number of cycles for a single cell with HA-45 and Nafion membranes is shown in Fig. 8. This decrease in capacity retention was 12.3% which was 87.7% for HA-45 whereas a drop of approximately 11.5% was seen for Nafion and it remained 88.5% after 50 cycles. The capacity to store charge always decreases during the discharge of a battery. This was mainly due to the crossing of the redox vanadium ion pair across the membrane. This low crossover of the VO^{2+} ion helps the redox pair to remain in their respective chambers, thus the capacity retention will be higher.

Table 3 shows the performance of the prepared membrane in terms of cell efficiency and vanadium permeability compared with membranes reported in the literature, under similar VRFB operating environments, which were comparable to the reported data[28,32,34,51–53]

4. Conclusion

DPVDF based St–DVB semi-interpenetrating network type membranes were successfully synthesized *via* free radical polymerization with various amounts of St and DVB followed by sulfonation using CSA. The HA-45 membrane showed low vanadium permeability with better ionic conductivity. The VRFB single cell performance for the HA-45 exhibits outstanding cell efficiency, in particular, an excellent CE of 93% and EE of 87%, due to the lower cell resistance. The HA-45 exhibited a peak power density of 336 mW cm^{-2} at a current density of 470 mA cm^{-2}. The HA-45 membrane possesses excellent specific capacity ranging from 20.30 A h L^{-1} to 21.11 A h L^{-1} at current densities of 50 mA cm^{-2} and 100 mA cm^{-2}, respectively, compared to the theoretical specific capacities of 26.8 A h L^{-1} for 1 M electrolyte solution. Because the VRFB operation time at 100 mA cm^{-2} is nearly half that at 50 mA cm^{-2}, the cumulative vanadium crossover was also reduced; therefore at 100 mA cm^{-2}, the specific capacity is 1.29 A h L^{-1} more than that at 50 mA cm^{-2}. The HA-45 membrane shows a similar pattern of charging and discharging in a single cell as the Nafion 117 membrane with equivalent energy efficiency. The results show that the HA-45 membrane is a suitable candidate for use in VRFB applications.

Conflicts of interest

There are no conflicts to declare.

Acknowledgements

VK is thankful to the Department of Science and Technology, New Delhi, (grant "INT/RUS/RFBR/P-348") for providing funds for this research. Author KR acknowledges funding through DST grant "DST/SERI/S9 (C)". CSIR is also acknowledged for providing fund under FTT scheme. The Authors are also thankful to the Analytical Discipline and Centralized Instrument facility, CSMCRI, Bhavnagar, for instrumental support.

References

1 Y. Zhou, L. Liu, Y. Shen, L. Wu, L. Yu, F. Liang and J. Xi, Carbon dots promoted vanadium flow batteries for all-climate energy storage, *Chem. Commun.*, 2017, **53**, 7565–7568.
2 B. Schwenzer, J. Zhang, S. Kim, L. Li, J. Liu and Z. Yang, Membrane Development for Vanadium Redox Flow Batteries, *ChemSusChem*, 2011, **4**, 1388–1406.
3 D. Chen, S. Wang, M. Xiao and Y. Meng, Preparation and properties of sulfonated poly(fluorenyl ether ketone) membrane for vanadium redox flow battery application, *J. Power Sources*, 2010, **195**, 2089–2095.
4 M. Skyllas-Kazacos, D. Kasherman, D. R. Hong and M. Kazacos, Characteristics and performance of 1 kW UNSW vanadium redox battery, *J. Power Sources*, 1991, **35**, 399–404.
5 M. Skyllas-Kazacos, M. H. Chakrabarti, S. A. Hajimolana, F. S. Mjalli and M. Saleem, Progress in Flow Battery Research and Development, *J. Electrochem. Soc.*, 2011, **158**, R55.
6 C. Wu, S. Lu, H. Wang, X. Xu, S. Peng, Q. Tan and Y. Xiang, A novel polysulfone–polyvinylpyrrolidone membrane with superior proton-to-vanadium ion selectivity for vanadium redox flow batteries, *J. Mater. Chem. A*, 2016, **4**, 1174–1179.
7 J. Kim, Y. Lee, J.-D. Jeon and S.-Y. Kwak, Ion-exchange composite membranes pore-filled with sulfonated poly(ether ether ketone) and Engelhard titanosilicate-10 for improved performance of vanadium redox flow batteries, *J. Power Sources*, 2018, **383**, 1–9.
8 S. Gahlot and V. Kulshrestha, Graphene based polymer electrolyte membranes for electrochemical energy applications, *Int. J. Hydrogen Energy*, 2020, **45**, 17029–17056.
9 J. Dai, Y. Dong, C. Yu, Y. Liu and X. Teng, A novel Nafion-g-PSBMA membrane prepared by grafting zwitterionic SBMA onto Nafion *via* SI-ATRP for vanadium redox flow battery application, *J. Membr. Sci.*, 2018, **554**, 324–330.
10 R. M. Darling, K. G. Gallagher, J. A. Kowalski, S. Ha and F. R. Brushett, Pathways to low-cost electrochemical energy storage: a comparison of aqueous and nonaqueous flow batteries, *Energy Environ. Sci.*, 2014, **7**, 3459–3477.
11 Z. Yang, J. Zhang, M. C. W. Kintner-Meyer, X. Lu, D. Choi, J. P. Lemmon and J. Liu, Electrochemical Energy Storage for Green Grid, *Chem. Rev.*, 2011, **111**, 3577–3613.
12 M. Skyllas-Kazacos, New All-Vanadium Redox Flow Cell, *J. Electrochem. Soc.*, 1986, **133**, 1057.
13 S. Zhang, C. Yin, D. Xing, D. Yang and X. Jian, Preparation of chloromethylated/quaternized poly(phthalazinone ether ketone) anion exchange membrane materials for vanadium redox flow battery applications, *J. Membr. Sci.*, 2010, **363**, 243–249.
14 Y. Li, J. Sniekers, J. C. Malaquias, C. Van Goethem, K. Binnemans, J. Fransaer and I. F. J. Vankelecom, Cross-linked anion exchange membranes prepared from poly(phenylene oxide) (PPO) for non-aqueous redox flow batteries, *J. Power Sources*, 2018, **378**, 338–344.
15 S. Muench, A. Wild, C. Friebe, B. Häupler, T. Janoschka and U. S. Schubert, Polymer-Based Organic Batteries, *Chem. Rev.*, 2016, **116**, 9438–9484.
16 S. Hameer and J. L. van Niekerk, A review of large-scale electrical energy storage, *Int. J. Energy Res.*, 2015, **39**, 1179–1195.
17 P. P. Sharma, A. Paul, D. N. Srivastava and V. Kulshrestha, Semi-Interpenetrating Network-Type Cross-Linked Amphoteric Ion-Exchange Membrane Based on Styrene Sulfonate and Vinyl Benzyl Chloride for Vanadium Redox Flow Battery, *ACS Omega*, 2018, **3**, 9872–9879.
18 W. Dai, Y. Shen, Z. Li, L. Yu, J. Xi and X. Qiu, SPEEK/Graphene oxide nanocomposite membranes with superior cyclability for highly efficient vanadium redox flow battery, *J. Mater. Chem. A*, 2014, **2**, 12423–12432.
19 M. Branchi, M. Gigli, B. Mecheri, F. Zurlo, S. Licoccia and A. D'Epifanio, Highly ion selective hydrocarbon-based membranes containing sulfonated hypercrosslinked polystyrene nanoparticles for vanadium redox flow batteries, *J. Membr. Sci.*, 2018, **563**, 552–560.
20 W. Y. Hsu and T. D. Gierke, Ion transport and clustering in Nafion perfluorinated membranes, *J. Membr. Sci.*, 1983, **13**, 307–326.
21 X. Li, H. Zhang, Z. Mai, H. Zhang and I. Vankelecom, Ion exchange membranes for vanadium redox flow battery (VRB) applications, *Energy Environ. Sci.*, 2011, **4**, 1147.
22 T. Mohammadi, S. C. Chieng and M. S. Kazacos, Water transport study across commercial ion exchange membranes in the vanadium redox flow battery, *J. Membr. Sci.*, 1997, **133**, 151–159.
23 Q. Luo, L. Li, W. Wang, Z. Nie, X. Wei, B. Li, B. Chen, Z. Yang and V. Sprenkle, Capacity Decay and Remediation of Nafion-based All-Vanadium Redox Flow Batteries, *ChemSusChem*, 2013, **6**, 268–274.
24 K. K. Jana, S. J. Lue, A. Huang, J. F. Soesanto and K.-L. Tung, Separator Membranes for High Energy-Density Batteries, *ChemBioEng Rev.*, 2018, **5**, 346–371.
25 P. P. Sharma, V. Yadav, S. Gahlot, O. V. Lebedeva, A. N. Chesnokova, D. N. Srivastava, T. V. Raskulova and V. Kulshrestha, Acid resistant PVDF-*co*-HFP based copolymer proton exchange membrane for electrochemical application, *J. Membr. Sci.*, 2019, **573**, 485–492.
26 Q. Zhang, Q.-F. Dong, M.-S. Zheng and Z.-W. Tian, The preparation of a novel anion-exchange membrane and its application in all-vanadium redox batteries, *J. Membr. Sci.*, 2012, **421–422**, 232–237.
27 S. Winardi, S. C. Raghu, M. O. Oo, Q. Yan, N. Wai, T. M. Lim and M. Skyllas-Kazacos, Sulfonated poly(ether ether ketone)-based proton exchange membranes for vanadium redox battery applications, *J. Membr. Sci.*, 2014, **450**, 313–322.
28 B. Yin, Z. Li, W. Dai, L. Wang, L. Yu and J. Xi, Highly branched sulfonated poly(fluorenyl ether ketone sulfone)s membrane for energy efficient vanadium redox flow battery, *J. Power Sources*, 2015, **285**, 109–118.
29 Y. Zhou, P. Qiu, Y. Ma, X. Zhang, D. Xu, J. Lin, Y. Tang, F. Wang, X. He, Z. Zhou, N. Sun and D. Sun, $BaTiO_3$/PVDF-g-PSSA composite proton exchange membranes for vanadium redox flow battery, *Ceram. Int.*, 2015, **41**, S758–S762.

30 P. P. Sharma, V. Yadav, S. Gahlot, O. V. Lebedeva, A. N. Chesnokova, D. N. Srivastava, T. V. Raskulova and V. Kulshrestha, Acid resistant PVDF-*co*-HFP based copolymer proton exchange membrane for electrochemical application, *J. Membr. Sci.*, 2019, **573**, 485–492.

31 Z. Mai, H. Zhang, X. Li, S. Xiao and H. Zhang, Nafion/polyvinylidene fluoride blend membranes with improved ion selectivity for vanadium redox flow battery application, *J. Power Sources*, 2011, **196**, 5737–5741.

32 Z. Li, J. Xi, H. Zhou, L. Liu, Z. Wu, X. Qiu and L. Chen, Preparation and characterization of sulfonated poly(ether ether ketone)/poly(vinylidene fluoride) blend membrane for vanadium redox flow battery application, *J. Power Sources*, 2013, **237**, 132–140.

33 J. Vrána, J. Charvát, P. Mazúr, P. Bělský, J. Dundálek, J. Pocedič and J. Kosek, Commercial perfluorosulfonic acid membranes for vanadium redox flow battery: Effect of ion-exchange capacity and membrane internal structure, *J. Membr. Sci.*, 2018, **552**, 202–212.

34 M. Bhushan, S. Kumar, A. K. Singh and V. K. Shahi, High-performance membrane for vanadium redox flow batteries: Crosslinked poly(ether ether ketone) grafted with sulfonic acid groups *via* the spacer, *J. Membr. Sci.*, 2019, **583**, 1–8.

35 S. Liu, L. Wang, Y. Ding, B. Liu, X. Han and Y. Song, Novel sulfonated poly(ether ether keton)/polyetherimide acid-base blend membranes for vanadium redox flow battery applications, *Electrochim. Acta*, 2014, **130**, 90–96.

36 A. Rajput, P. P. Sharma, V. Yadav and V. Kulshrestha, Highly stable graphene oxide composite proton exchange membrane for electrochemical energy application, *Int. J. Hydrogen Energy*, 2020, **45**, 16976–16983.

37 L. Su, D. Zhang, S. Peng, X. Wu, Y. Luo and G. He, Orientated graphene oxide/Nafion ultra-thin layer coated composite membranes for vanadium redox flow battery, *Int. J. Hydrogen Energy*, 2017, **42**, 21806–21816.

38 X. Teng, J. Dai, J. Su and G. Yin, Modification of Nafion membrane using fluorocarbon surfactant for all vanadium redox flow battery, *J. Membr. Sci.*, 2015, **476**, 20–29.

39 J. Kim, J.-D. Jeon and S.-Y. Kwak, Nafion-based composite membrane with a permselective layered silicate layer for vanadium redox flow battery, *Electrochem. Commun.*, 2014, **38**, 68–70.

40 S. Pal, R. Mondal, S. Guha, U. Chatterjee and S. K. Jewrajka, Homogeneous phase crosslinked poly(acrylonitrile-*co*-2-acrylamido-2-methyl-1-propanesulfonic acid) conetwork cation exchange membranes showing high electrochemical properties and electrodialysis performance, *Polymer*, 2019, **180**, 121680.

41 V. Pasala, J. N. Ramavath, C. He, V. K. Ramani and K. Ramanujam, N- and P-*co*-doped Graphite Felt Electrode for Improving Positive Electrode Chemistry of the Vanadium Redox Flow Battery, *ChemistrySelect*, 2018, **3**, 8678–8687.

42 A. Rajput, V. Yadav, P. P. Sharma and V. Kulshrestha, Synthesis of SGO composite interpenetrating network (CIPN) cation exchange membranes: Stability and salt removal efficiency, *J. Membr. Sci.*, 2018, **564**, 44–52.

43 S. Kumar, M. Bhushan and V. K. Shahi, Crosslinked amphoteric membrane: Sulphonated poly(ether ether ketone) grafted with 2,4,6-tris(dimethylaminomethyl)phenol using functionalized side chain spacers for vanadium redox flow battery, *J. Power Sources*, 2020, **448**, 227358.

44 H. Pei, W. Guo, R. Guo, Y. Li, C. Fang, Y. Zhang, W. Liu, Y. Wang and J. Xie, The Stability of Polymers in Liquid Li-S Battery, *J. Electrochem. Soc.*, 2019, **166**, A5215–A5220.

45 S. Gahlot and V. Kulshrestha, Dramatic Improvement in Water Retention and Proton Conductivity in Electrically Aligned Functionalized CNT/SPEEK Nanohybrid PEM, *ACS Appl. Mater. Interfaces*, 2015, **7**, 264–272.

46 S. Gahlot and V. Kulshrestha, White graphene based composite proton exchange membrane: Improved durability and proton conductivity, *Int. J. Hydrogen Energy*, 2018, **43**, 21683–21689.

47 M. Vijayakumar, Q. Luo, R. Lloyd, Z. Nie, X. Wei, B. Li, V. Sprenkle, J. D. Londono, M. Unlu and W. Wang, Tuning the Perfluorosulfonic Acid Membrane Morphology for Vanadium Redox-Flow Batteries, *ACS Appl. Mater. Interfaces*, 2016, **8**, 34327–34334.

48 I. S. Chae, T. Luo, G. H. Moon, W. Ogieglo, Y. S. Kang and M. Wessling, Ultra-High Proton/Vanadium Selectivity for Hydrophobic Polymer Membranes with Intrinsic Nanopores for Redox Flow Battery, *Adv. Energy Mater.*, 2016, **6**, 1600517.

49 J. Vrána, J. Charvát, P. Mazúr, P. Bělský, J. Dundálek, J. Pocedič and J. Kosek, Commercial perfluorosulfonic acid membranes for vanadium redox flow battery: Effect of ion-exchange capacity and membrane internal structure, *J. Membr. Sci.*, 2018, **552**, 202–212.

50 J. Xi, Z. Wu, X. Qiu and L. Chen, Nafion/SiO_2 hybrid membrane for vanadium redox flow battery, *J. Power Sources*, 2007, **166**, 531–536.

51 W. Wei, H. Zhang, X. Li, Z. Mai and H. Zhang, Poly(tetrafluoroethylene) reinforced sulfonated poly(ether ether ketone) membranes for vanadium redox flow battery application, *J. Power Sources*, 2012, **208**, 421–425.

52 W. Dai, Y. Shen, Z. Li, L. Yu, J. Xi and X. Qiu, SPEEK/Graphene oxide nanocomposite membranes with superior cyclability for highly efficient vanadium redox flow battery, *J. Mater. Chem. A*, 2014, **2**, 12423–12432.

53 Z. Li, W. Dai, L. Yu, L. Liu, J. Xi, X. Qiu and L. Chen, Properties Investigation of Sulfonated Poly(ether ether ketone)/Polyacrylonitrile Acid–Base Blend Membrane for Vanadium Redox Flow Battery Application, *ACS Appl. Mater. Interfaces*, 2014, **6**, 18885–18893.

